D1-Asn-298 in photosystem II is involved in a hydrogen-bond network near the redox-active tyrosine Y_Z for proton exit during water oxidation

Received for publication, August 29, 2017, and in revised form, October 4, 2017 Published, Papers in Press, October 18, 2017, DOI 10.1074/jbc.M117.815183

Ryo Nagao[1], **Hanayo Ueoka-Nakanishi, and Takumi Noguchi**[2]

From the Division of Material Science, Graduate School of Science, Nagoya University, Furo-cho, Chikusa-ku, Nagoya 464-8602, Japan

Edited by Joseph Jez

In photosynthetic water oxidation, two water molecules are converted into one oxygen molecule and four protons at the Mn_4CaO_5 cluster in photosystem II (PSII) via the S-state cycle. Efficient proton exit from the catalytic site to the lumen is essential for this process. However, the exit pathways of individual protons through the PSII proteins remain to be identified. In this study, we examined the involvement of a hydrogen-bond network near the redox-active tyrosine Y_Z in proton transfer during the S-state cycle. We focused on spectroscopic analyses of a site-directed variant of D1-Asn-298, a residue involved in a hydrogen-bond network near Y_Z. We found that the D1-N298A mutant of *Synechocystis* sp. PCC 6803 exhibits an O_2 evolution activity of ~10% of the wild-type. D1-N298A and the wild-type D1 had very similar features of thermoluminescence glow curves and of an FTIR difference spectrum upon Y_Z oxidation, suggesting that the hydrogen-bonded structure of Y_Z and electron transfer from the Mn_4CaO_5 cluster to Y_Z were little affected by substitution. In the D1-N298A mutant, however, the flash-number dependence of delayed luminescence showed a monotonic increase without oscillation, and FTIR difference spectra of the S-state cycle indicated partial and significant inhibition of the $S_2 \rightarrow S_3$ and $S_3 \rightarrow S_0$ transitions, respectively. These results suggest that the D1-N298A substitution inhibits the proton transfer processes in the $S_2 \rightarrow S_3$ and $S_3 \rightarrow S_0$ transitions. This in turn indicates that the hydrogen-bond network near Y_Z can be functional as a proton transfer pathway during photosynthetic water oxidation.

Plants and cyanobacteria utilize water as an ultimate electron donor to reduce carbon dioxide in the synthesis of sugars (1). This reaction of water oxidation is performed in photosystem II (PSII)[3] protein complexes, which are embedded in thylakoid membranes. Water oxidation produces protons and molecular oxygen (2–9); protons are released into the thylakoid lumen, making a proton gradient across the membrane, and are used to synthesize ATP, whereas molecular oxygen is liberated to the air to be the major oxygen source of the atmosphere.

In PSII, photochemical reactions start with light-induced charge separation between the primary donor chlorophyll (Chl), P680, and the pheophytin electron acceptor, Pheo (10, 11). An electron is transferred from Pheo to the primary quinone electron acceptor, Q_A, and then the secondary quinone electron acceptor, Q_B (12). On the electron donor side, the P680 cation abstracts an electron from the redox-active tyrosine, Y_Z (D1-Tyr-161), which immediately becomes a neutral radical ($Y_Z^{\bullet}$) by shifting a proton to the neighboring D1-His-190 through a strong hydrogen bond, forming a protonated His cation (13–16). $Y_Z^{\bullet}$ then oxidizes the water-oxidizing center (WOC), the catalytic site of water oxidation, which consists of a Mn_4CaO_5 cluster as an inorganic core, its amino acid (D1-Asp-170, D1-Glu-189, D1-His-332, D1-Glu-333, D1-Asp-342, D1-Ala-344, and CP43-Glu-354) and water (W1–W4) ligands, two Cl ions (Cl-1 and Cl-2), a hydrogen-bonded network formed by nearby water molecules and amino acid residues (Fig. 1*A*) (17–21). The water-oxidation reaction proceeds by a light-driven cycle of five intermediates, called S_i-state ($i = 0–4$; with a larger i value representing a higher oxidation state), in which the one-electron-oxidized S_1-state is the most stable in the dark (Fig. 1*B*) (22–23). Each S-state advances to the next state upon one-electron oxidation, except that the S_4-state, which is the most oxidized but unstable intermediate, immediately relaxes to the S_0-state, by releasing an O_2 molecule (2–9). During this S-state cycle, four protons are released to the lumen with a stoichiometry of 1:0:1:2 for the $S_0 \rightarrow S_1$:$S_1 \rightarrow S_2$:$S_2 \rightarrow S_3$:$S_3 \rightarrow S_0$ transitions (24–26). Because no proton is released in the $S_1 \rightarrow S_2$ transition, an excessive positive charge is accumulated on the Mn_4CaO_5 cluster in the S_2- and S_3-states.

Efficient proton exit from the catalytic site is essential in the mechanism of water oxidation. However, it remains unclear how the four protons are transferred from WOC to the lumen through the PSII proteins during the S-state cycle. The X-ray

This work was supported by the Grants-in-Aid for Scientific Research from Japan Society for the Promotion of Science 26840091 and 17K07442 (to R. N.) and 17H03662 and 17H06435 (to T. N.). The authors declare that they have no conflicts of interest with the contents of this article.

[1] To whom correspondence may be addressed: Research Institute for Interdisciplinary Science, Okayama University, 3-1-1 Tsushima-naka, Okayama 700-8530, Japan. Tel.: 81-86-251-8630; Fax: 81-86-251-8630; E-mail: nagaoryo@okayama-u.ac.jp.

[2] To whom correspondence may be addressed. Tel: 81-52-789-2881; Fax: 81-52-789-2883; E-mail: tnoguchi@bio.phys.nagoya-u.ac.jp.

[3] The abbreviations used are: PSII, photosystem II; Chl, chlorophyll; DCBQ, 2,6-dichloro-*p*-benzoquinone; DL, delayed luminescence; DM, *n*-dodecyl β-D-maltoside; MD, molecular dynamics; QM/MM, quantum mechanics/molecular mechanics; TL, thermoluminescence; DCMU, 3-(3,4)-dichlorophenyl-1,1-dimethylurea; Km, kanamycin; Cm, chloramphenicol; Em, erythromycin; Sm, spectinomycin.

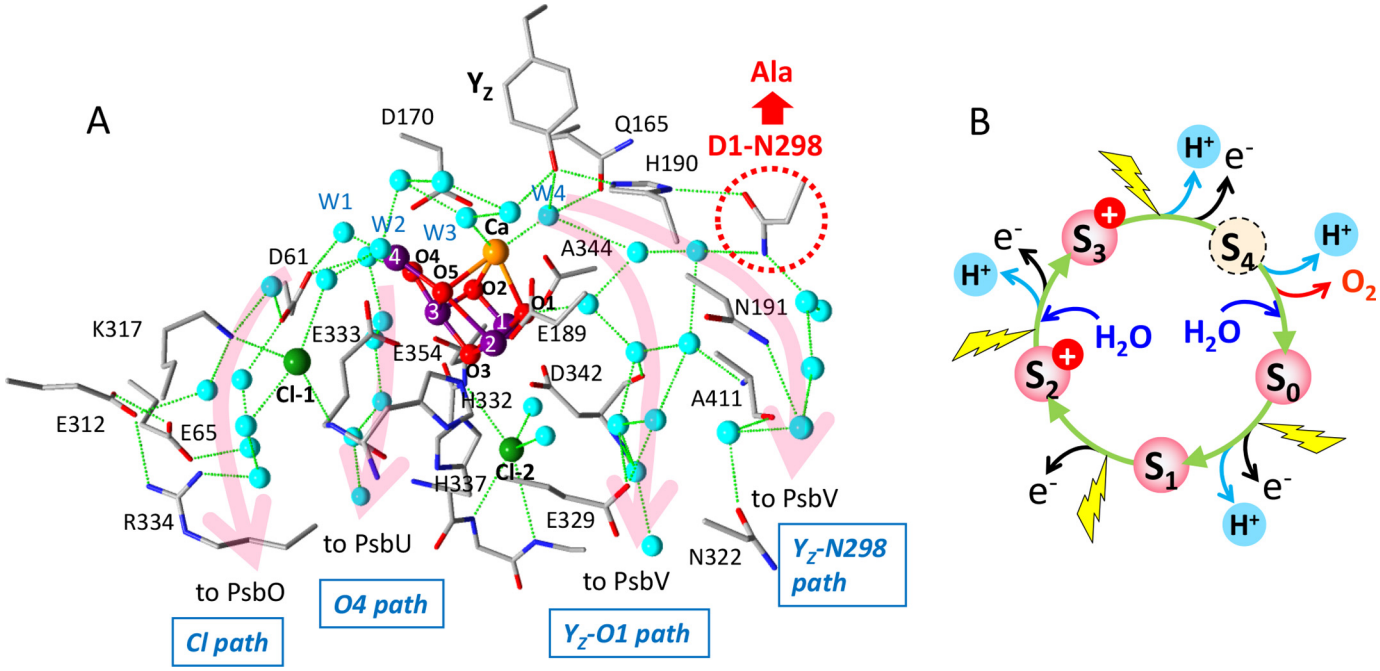

Figure 1. *A,* hydrogen-bond network around the Mn_4CaO_5 cluster and putative proton transfer pathways. The X-ray free electron laser structure of *Thermosynechococcus vulcanus* at 1.95-Å resolution (PDB code 4UB6 (18)) was used to draw the picture. Mn, *purple*; Ca, *orange*; Cl, *green*; O, *red*; N, *blue*. Oxygen atoms of water molecules are colored *cyan*. The numbering of the Mn and oxygen atoms in the Mn_4CaO_5 cluster and its water ligands follows the numbering in Umena *et al.* (17). D1-Asn-298, which was replaced with Ala in this work, is *circled with a red dotted line*. *Magenta arrows* represent putative proton pathways, which were designated Cl path, O4 path, Y_Z-O1 path, and Y_Z-Asn-298 path in this work. Hydrogen bonds are shown with *green dotted lines*. Amino acid residues with labels are on the D1 subunit except for Lys-317 and Glu-312 on the D2 subunit, and Glu-354 and Ala-411 on the CP43 subunit. *B,* the S-state cycle of water oxidation.

structures of PSII complexes (17, 18, 27, 28) and theoretical calculations based on them have shown that there are several channels suitable for proton transfer around the Mn_4CaO_5 cluster leading to the lumen (Fig. 1*A*) (29–39). These channels involve a number of water molecules forming hydrogen-bond networks, as revealed by the recent high-resolution X-ray structures that resolved water oxygen atoms (17–21). Near the entrance of each channel, either D1-Asp-61 or Y_Z is located, and a water cluster is formed between these two residues including water ligands to Mn4 (W1 and W2) and Ca^{2+} (W3 and W4).

The channel from D1-Asp-61 to PsbO through the Cl-1 site and the D1-Glu-65/D2-Glu-312/D1-Arg-334 triad has been most extensively studied and proposed to function as a pathway for protons or substrate water (designated "Cl path" in the present report; Fig. 1*A*) (29–37, 39). Theoretical calculations suggested that D1-Asp-61 plays a crucial role in proton transfer (40, 41), and that the Cl^- ion has a function to regulate proton transfer through this pathway (34). D1-Asp-61 is also located near the entrance of a water chain starting at O4 and leading to PsbU (designated "O4 path"; Fig. 1*A*), which has been proposed to function as a proton exit pathway especially in the $S_0 \rightarrow S_1$ transition (38, 39). The recent X-ray free electron laser study for the S_3-state showed the displacement of a water molecule near O4, suggesting the involvement of water molecules near O4 in proton transfer (21). The hydrogen-bond network near Y_Z has also been suggested to be a proton pathway (16, 17, 42, 43). Y_Z form a hydrogen-bonded triad with D1-His-190 and D1-Asn-298, which is connected with a hydrogen-bond network leading to PsbV through D1-Asn-322 (designated "Y_Z-Asn-298 path"; Fig. 1*A*). Molecular dynamics (MD) simulations (36, 39) suggested a tight hydrogen-bond network of this pathway, which is advantageous to proton transfer. A large water cluster interacting the Y_Z/D1-His-190/D1-Asn-298 triad also forms another hydrogen-bond network through O1 and D1-Glu-329 leading to PsbV (designated "Y_Z-O1 path"). MD simulation showed that this channel contains a number of mobile water molecules (33, 39). It is noted that the above key amino acid residues in the hydrogen-bond networks in cyanobacterial PSII (Fig. 1*A*) are all conserved in higher plants whose PSII-LHCII structures were recently resolved by cryo-electron microscopy (44, 45).

The finding of several channels around the Mn_4CaO_5 cluster raises a question, which proton pathways are used for individual protons released in the S-state transitions? The most direct experimental method to answer this question is examining the effects of site-directed mutations, by which amino acid residues on putative proton channels are altered to different amino acids, on the reactions of individual S-state transitions. Many mutants of amino acid residues in putative channels have been investigated so far (46–60). Most of them are located on the Cl path; mutations of D1-Asp-61 to Ala and Asn significantly retarded the kinetic rate of O_2 release in the $S_3 \rightarrow S_0$ transition (47, 53, 58) and changed the property of a nearby water network (57). Mutations of D2-Lys-317 and D1-Asn-181, which are ligands to Cl-1, also retarded the O_2 kinetics or decreased the efficiency of the $S_3 \rightarrow S_0$ transition (54, 55, 59). In addition, mutants of any of the D1-Glu-65/D2-Glu-312/D1-Arg-334 triad substantially inhibited the $S_3 \rightarrow S_0$ transition (49, 52). These data suggest that the Cl path is involved in proton or water transfer at least in the $S_3 \rightarrow S_0$ transition, although a caution is necessary in the interpretation of results for charged residues, whose mutations could affect the redox potential of

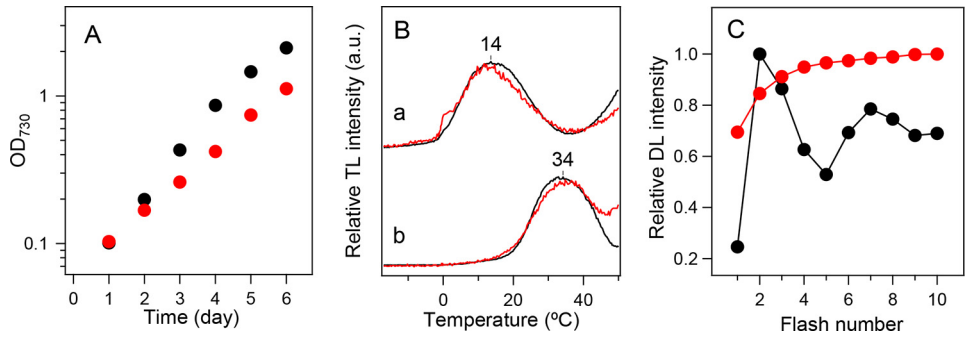

Figure 2. *In vivo* characterization of WT* (*black*) and D1-N298A (*red*) cells. *A*, growth curves of cells. *B*, TL glow curves in the (*a*) presence and (*b*) absence of DCMU representing charge recombination of the $S_2Q_A^-$ and $S_2Q_B^-$ charged pairs, respectively. *C*, flush-number dependence of DL induced by 10 successive flashes (1 Hz). DL was measured at 25 °C and the amplitude at 0.8 s after each flash was plotted.

the Mn_4CaO_5 cluster and hence the electron transfer reaction. In contrast, fewer mutagenesis studies have been performed for the channels near the Y_Z site. Mutation of D1-Gln-165, which is hydrogen-bonded with W4 near Y_Z, to Glu decreased the efficiency of the $S_3 \rightarrow S_0$ transition (56), whereas mutation of D1-Glu-329 on the Y_Z-O1 path to Gln little affected the S-state transitions (52). Fourier transform infrared (FTIR) analysis of the S-state cycle using various mutants by Debus and co-workers (52, 54, 56, 57) further showed the presence of an extensive hydrogen-bond network around the Mn_4CaO_5 cluster.

D1-Asn-298 is located at a crucial position to keep a hydrogen-bond network involving water molecules in the Y_Z-Asn-298 and Y_Z-O1 pathways (Fig. 1*A*). This has also been proposed to be a key residue to determine the hydrogen-bonded structure of Y_Z and the rate of its proton-coupled electron transfer through the interaction with D1-His-190 (15, 16). Thus, mutation of D1-Asn-298 could affect the proton transfer from the catalytic site as well as electron transfer from the Mn_4CaO_5 cluster to $Y_Z^{\bullet}$ during S-state transitions. Yamasato *et al.* (50) previously found that the D1-N298I mutant obtained by random mutagenesis inhibited electron flow from water to the electron acceptor side. More recently, Kuroda *et al.* (60) generated 19 site-directed mutants of D1-Asn-298 using *Chlamydomonas reinhardtii*, and showed that only seven mutants (D1-N298G, -A, -C, -M, -S, -Q, and -H) have O_2 evolution activity but with significantly low rates. However, detailed properties of the mutants of D1-Asn-298, such as specific inhibition of either electron or proton transfer in individual S-state transitions, have not yet been investigated, and hence no clear answer was obtained about the involvement of pathways near the Y_Z site in the water oxidation mechanism.

In this work, we investigated whether the hydrogen-bond network near Y_Z is functional or not in proton transfer during water oxidation, by constructing a D1-N298A mutant using a cyanobacterium *Synechocystis* sp. PCC 6803, and analyzing this mutant by means of light-induced FTIR difference spectroscopy and detection of thermoluminescence (TL) and delayed luminescence (DL). Because Asn and Ala are both non-charged amino acids and the replacement with a small Ala side chain can avoid the undesirable alterations of main chains, only the perturbation of the hydrogen-bond network is expected to occur without changes in the electrostatic interaction and protein conformations. FTIR difference spectroscopy is a powerful method for detecting the structural perturbations of amino acid residues, water molecules, and the hydrogen-bond network around the Mn_4CaO_5 cluster, as well as monitoring the inhibition of the S-state transitions (61–70). The results provided solid evidence for the involvement of D1-Asn-298, and hence the hydrogen-bond network near Y_Z, in proton transfer in the $S_2 \rightarrow S_3$ and $S_3 \rightarrow S_0$ transitions of water oxidation.

Results

In vivo analyses of the D1-N298A mutant

The strains of *Synechocystis* sp. PCC 6803 used in the present study lacked the *psbA1* and *psbA3* genes, and hence PsbA2 was expressed as a D1 protein (71). In addition, a histidine tag was attached to the C terminus of the CP47 protein. Thus, the strain having a PsbA2 protein with a native sequence is designated "WT*" hereafter. In contrast, the Asn-298 of PsbA2 was replaced by Ala in the D1-N298A mutant. The D1-N298A mutant grew photoautotrophically with a rate slightly slower than the WT* (Fig. 2*A*). The O_2 evolution activities of WT* and D1-N298A were 600–670 and 60–70 μmol of O_2 (mg of Chl)$^{-1}$ h^{-1}, respectively, in cells, and 2800–3300 and 190–300 μmol of O_2 (mg of Chl)$^{-1}$ h^{-1}, respectively, in isolated PSII complexes. Thus, the O_2 evolution activity of the D1-N298A mutant is about 10% of WT* in both cells and PSII core complexes. This reduced activity of the D1-N298A mutant is in good agreement with that of a corresponding mutant of a green alga *C. reinhardtii*, which showed a 11.5% activity of WT in cells (60).

TL glow curves of PSII in the presence and absence of DCMU originate from charge recombination of $S_2Q_A^-$ (Q band) and $S_2Q_B^-$ (B band), respectively (72). WT* cells showed Q and B bands at about 14 and 34 °C, respectively, and they were virtually unaffected by the D1-N298A mutation (Fig. 2*B*). In contrast, the flash-number dependence of DL, which was monitored at 0.8 s after each flash, showed significantly different patterns between WT* and D1-N298A cells (Fig. 2*C*). Whereas WT* cells showed a typical period-four oscillation of DL signals, D1-N298A cells did not show any oscillation and the DL amplitude monotonically increased with a flash number.

FTIR difference spectrum upon Y_Z oxidation

Light-induced FTIR difference spectra upon Y_Z oxidation ($Y_Z^{\bullet}/Y_Z$ difference spectra) were obtained using manganese-depleted PSII core complexes of WT* and D1-N298A (Fig. 3). Characteristic bands of the $Y_Z^{\bullet}/Y_Z$ spectra were virtually iden-

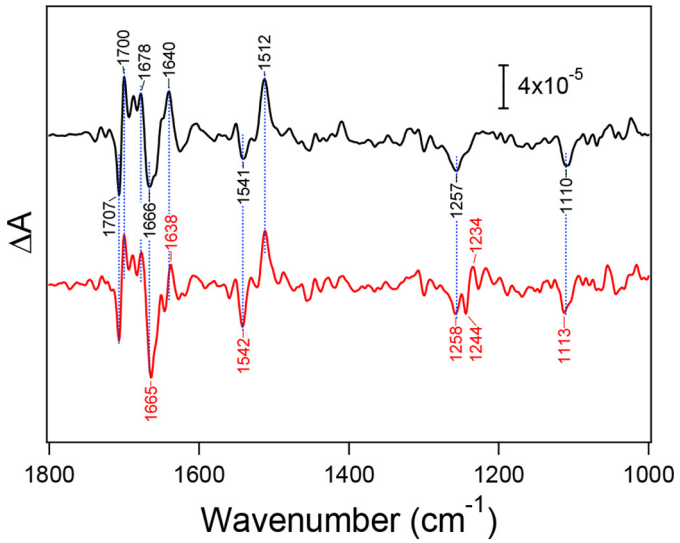

Figure 3. Flash-induced FTIR difference spectra upon Y_Z oxidation of manganese-depleted PSII core complexes from WT* (*black line*) and D1-N298A (*red line*). Spectra were measured at 250 K. The spectrum of D1-N298A was scaled to adjust the intensity of the ferricyanide CN peak at 2116 cm^{-1} (not shown) to that in the WT* spectrum.

tical between the two species. The prominent positive band at 1512 cm^{-1} has been assigned to the CO stretching vibration of the oxidized $Y_Z^{\bullet}$ radical, whereas a negative band at 1258–1257 cm^{-1} has been assigned to the coupled CO stretching/COH bending vibration of neutral Y_Z (16, 73). A differential signal at 1707/1700 cm^{-1} and a negative peak at 1113–1110 cm^{-1} have been attributed to the keto C = O vibration of P_{D1} in P680 affected by Y_Z oxidation (71) and the imidazole CN stretch of D1-His-190 hydrogen bonded with Y_Z (73), respectively. Bands in the 1680–1630 cm^{-1} region, and a band at 1541 cm^{-1} can be assigned to amide I and II vibrations, respectively, representing the perturbations of protein backbones. Except for changes in other minor bands and some intensity changes in the amide I and II bands, a notable change by the mutation was observed only in the appearance of a differential signal at 1244/1234 cm^{-1} in the spectrum of D1-N298A, although the origin of this signal is unknown at the present stage. The absence of significant changes in the characteristic bands upon the D1-N298A mutation indicates that the hydrogen-bonded interaction of Y_Z was virtually unaffected by this mutation.

Flash-induced FTIR difference spectra of S-state transitions

Light-induced FTIR difference spectra of the S-state cycle of WOC were measured by applying four flashes on the O_2-evolving PSII core complexes from WT* and D1-N298A. The first-, second-, third-, and fourth-flash spectra of the WT* PSII complexes in a moderately hydrated film (Fig. 4*A*, *black lines*) represent the structural changes upon the $S_1 \rightarrow S_2$, $S_2 \rightarrow S_3$, $S_3 \rightarrow S_0$, and $S_0 \rightarrow S_1$ transitions, respectively. The spectral features were very similar to those of previously reported spectra (52, 54–57, 74–81). Bands at 1700–1600 cm^{-1} mainly arise from the amide I vibrations (CO stretching vibrations of backbone amides), representing the perturbations of polypeptide chains near the Mn_4CaO_5 cluster (78, 82). Characteristic bands at 1450–1350 cm^{-1} are due to the symmetric COO^- stretching vibrations (78, 80–85), whereas the coupled asymmetric

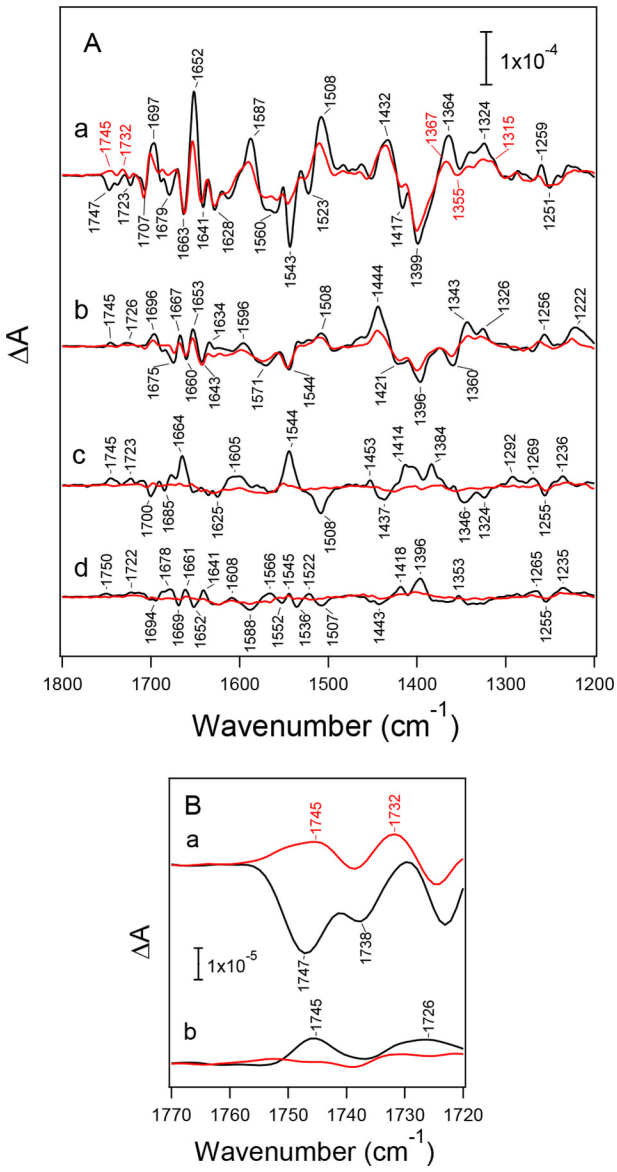

Figure 4. Flash-induced FTIR difference spectra of the S-state cycle of PSII core complexes from WT* (*black lines*) and D1-N298A (*red lines*) in moderately hydrated films. *A*, mid-infrared region (1800–1200 cm^{-1}) of protein vibrations. Difference spectra were measured upon the (*a*) first, (*b*) second, (*c*) third, and (*d*) fourth flashes. *B*, expanded view of the C = O stretching region of COOH groups (1770–1720 cm^{-1}) at the (*a*) first and (*b*) second flashes. The spectra of D1-N298A were scaled with a factor to adjust the intensity of the ferricyanide CN peak at 2116 cm^{-1} (not shown) in the first-flash spectrum to that of WT*.

COO^- stretching bands appear at 1600–1500 cm^{-1}, overlapping the amide II bands (NH bending and CN stretching vibrations of backbone amides) (78, 82). The changes of these COO^- bands during the S-state cycle are attributed to the structural changes of carboxylate residues around the Mn_4CaO_5 cluster (80, 81, 83–85). The obtained spectra showed characteristic features depending on the flash number, especially in the symmetric COO^- region around 1400 cm^{-1}, reflecting high efficiencies of the S-state transitions.

Spectra of the S-state cycle of the D1-N298A mutant at the first to fourth flashes are also shown in Fig. 4*A* (*red lines*) superimposing those of WT* (*black lines*). These spectra of D1-N298A were scaled using a factor to adjust the intensity of

the CN band of ferricyanide at 2116 cm^{-1} at the first-flash (not shown) to that of WT*, representing the same extent of an electron flow in PSII in the $S_1 \rightarrow S_2$ transition. Although the first-flash spectrum due to the $S_1 \rightarrow S_2$ transition showed overall features similar to those of WT*, some differences were observed in several bands (Fig. 4*A*, *a*). In the symmetric COO^- region, band intensities at 1417(−) and 1364(+) cm^{-1} were significantly reduced. In addition, bands at 1652(+), 1587(+), 1543(−), 1523(−), and 1508(+) cm^{-1} in the amide I and the asymmetric COO^-/amide II regions decreased their intensities. Furthermore, a negative band at 1747 cm^{-1}, which has been assigned to the C = O stretching vibration of an unidentified COOH group involved in a hydrogen-bond network around the Mn_4CaO_5 cluster (52, 56), diminished and is replaced by a positive band at 1745 cm^{-1} (Fig. 4*B*, *a*). In contrast, spectral features of the second-flash spectra of D1-N298A were very similar to those of WT* (Fig. 4Ab). However, an overall intensity in the COO^- region (1450–1300 cm^{-1}) was ~60% of WT*. A small positive peak at 1745 cm^{-1} due to a COOH group, which has a different origin from the negative band at 1747 cm^{-1} at the first flash (56), also diminished (Fig. 4*B*, *b*).

The most striking change in the spectra of the D1-N298A mutant is that the third- and fourth-flash spectra showed very small intensities (Fig. 4*A*, *c* and *d*), indicating that the $S_3 \rightarrow S_0$ transition was significantly inhibited in this mutant. Assuming that the FTIR spectrum of the $S_3 \rightarrow S_0$ transition in the D1-N298A mutant has an identical feature with that of WT*, spectral fitting in the COO^- region of the third-flash spectrum of the mutant using the second- and third-flash spectra of WT* (76) provided the ~20% contribution of the $S_3 \rightarrow S_0$ transition at the third flash. With the ~60% contribution of the $S_2 \rightarrow S_3$ transition at the second flash, it follows that the efficiency of the $S_3 \rightarrow S_0$ transition in the D1-N298A mutant is ~30% of WT*. Previously, the D2-K317R mutant also showed similar intensity decreases in the third- and fourth-flash FTIR spectra in a moderately hydrated film (55), but the intensities recovered in a solution sample. It was suggested that partial dehydration reduced the efficiency of the $S_3 \rightarrow S_0$ transition in the K317R mutant (55). To examine the similar dehydration effect, FTIR spectra of the S-state cycle were measured in solution samples of WT* and D1-N298A (Fig. 5). All the spectral changes by the D1-N298A mutation mentioned above were also observed in the solution samples, indicating that these changes are not ascribed to partial dehydration but are attributed to direct effects of the D1-N298A mutation irrespective of sample conditions.

The mutation effects were also observed in water vibrations obtained in hydrated PSII films. In the high frequency region of 3700–3500 cm^{-1} (Fig. 6*A*), weakly hydrogen-bonded OH vibrations of water molecules (77, 86, 87) showed a differential signal at 3607/3588 cm^{-1} and a negative band at 3662 cm^{-1} in the first-flash spectrum of WT*, analogously to the previous reports (57, 77, 80, 86, 87). In the D1-N298A mutant, the negative peak at 3662 cm^{-1} diminished, whereas another negative peak at 3588 cm^{-1} seems unchanged (Fig. 6*A*, *a*). At the second flash, a broad negative band at ~3620 cm^{-1} in WT* (57, 77) seemed slightly downshifted upon the D1-N298A mutation (Fig. 6*A*, *b*).

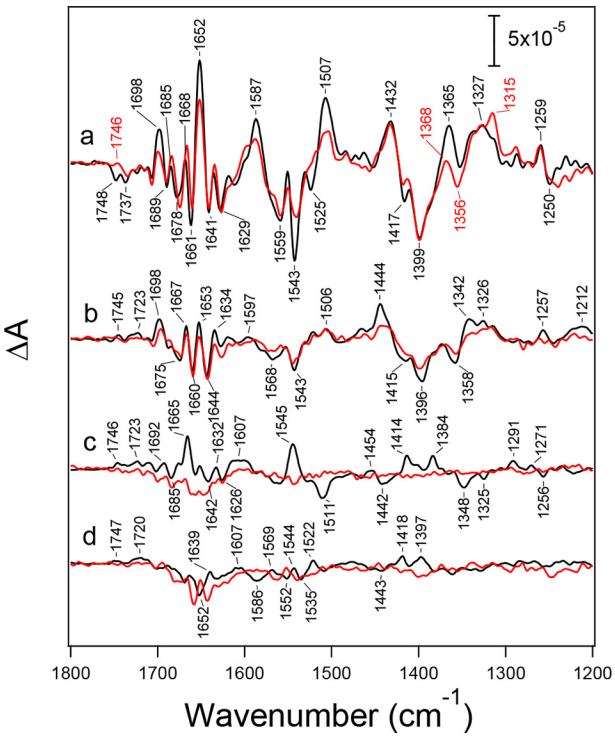

Figure 5. Flash-induced FTIR difference spectra (1800–1200 cm^{-1}) of the S-state cycle of PSII core complexes from WT* (*black lines*) and D1-N298A (*red lines*) in solutions measured upon the (*a*) first, (*b*) second, (*c*) third, and (*d*) fourth flashes. The spectra of D1-N298A were scaled with a factor to adjust the intensity of the ferricyanide CN peak at 2116 cm^{-1} (not shown) in the first-flash spectrum to that of WT*.

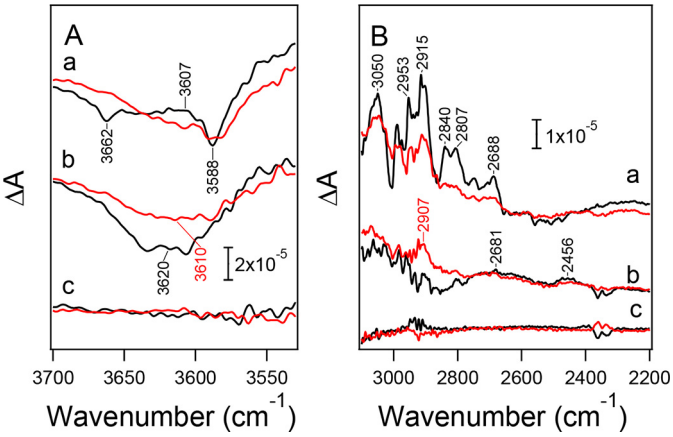

Figure 6. Flash-induced FTIR difference spectra of PSII core complexes from WT* (*black lines*) and D1-N298A (*red lines*) in moderately hydrated films in the regions of (*A*) weakly hydrogen-bonded OH vibrations of water (3700–3530 cm^{-1}) and (*B*) strongly hydrogen-bonded OH/NH vibrations (3100–2200 cm^{-1}). *a*, first flash; *b*, second flash; *c*, dark-minus-dark difference spectra representing noise levels. The intensities of the spectra of D1-N298A were scaled with the same factor as the corresponding spectra in Fig. 4. Signals around 2350 cm^{-1} in *panel B* are artifacts by CO_2 absorption.

In the region of vibrations of polarizable protons in strong hydrogen bonds (3100–2200 cm^{-1}) (77, 87), a broad positive feature with several sharp peaks was observed in the first-flash spectrum of WT* (Fig. 6*B*, *a*). This band feature was attributed to the OH stretching vibrations of water molecules around the Mn_4CaO_5 cluster (87), overlapping the NH stretching vibration with Fermi resonance peaks of a His side chain (D1-His-337)

hydrogen-bonded with the O3 oxo bridge of the Mn_4CaO_5 cluster (88). The intensities of these bands were weakened upon the D1-N298A mutation. In the second-flash spectra (Fig. 6*B, b*), WT* exhibited broad positive features at 2681 and 2456 cm^{-1} (57, 77), whereas a new positive band appeared at 2907 cm^{-1} upon the D1-N298A mutation leaving the broad features.

Discussion

D1-Asn-298 is a crucial amino acid residue in retaining a hydrogen-bond network near Y_Z. It supports a water chain that leads from W4 to PsbV through D1-Asn-191 and D1-Asn-322 (Y_Z-Asn-298 path), and a water cluster that interacts with O1 of the Mn_4CaO_5 cluster and D1-Glu-329 leading to PsbV (Y_Z-O1 path) (Fig. 1*A*), both of which have been candidates of proton/water pathways (31–33, 35–37, 39). Thus, mutation of D1-Asn-298 to non-hydrogen bonding Ala is expected to significantly perturb the structures of these hydrogen-bond networks by reorganizing nearby water molecules. In addition, D1-Asn-298 is a key amino acid residue in determining the hydrogen-bonded structure of Y_Z. The amide C = O of the Asn-298 side chain accepts an hydrogen bond from the Nπ-H of D1-His-190, whereas the Nτ of His-190 functions as a hydrogen-bond acceptor of the OH of Y_Z (15–18). This hydrogen-bonded structure of the Y_Z/D1-His-190/D1-Asn-298 triad realizes rapid proton-coupled electron transfer of Y_Z, in which upon oxidation by $P680^+$, the proton of Y_Z is immediately shifted to D1-His-190 forming a $HisH^+$ cation (15, 16). The D1-N298A mutation hence could also perturb the hydrogen-bonded structure of Y_Z and its reaction. In contrast, mutation from Asn to Ala, both of which are non-charged amino acids, should have little electrostatic effect on Y_Z and the Mn_4CaO_5 cluster to change their redox potentials. Furthermore, a relatively remote location (>10 Å) of D1-Asn-298 from the Mn_4CaO_5 cluster without any direct interactions even with the first shell ligands makes less likely the possibility that its mutation has a direct effect on the catalytic reaction of water oxidation.

We examined the effect of the D1-N298A mutation on the hydrogen-bonded structure of Y_Z by comparing the $Y_Z^{\bullet}/Y_Z$ FTIR difference spectrum of the manganese-depleted PSII core complex from the D1-N298A mutant with that from WT*. The results showed that they had very similar features (Fig. 3). In particular, the vibrational frequencies of the CO stretching band of $Y_Z^{\bullet}$ (1512 cm^{-1}) and the CO stretching/COH bending band of neutral Y_Z (1257 cm^{-1}), which are sensitive to changes in hydrogen-bonding interactions, were identical within 1 cm^{-1}, indicating that the hydrogen-bonded interaction of Y_Z was little affected by this mutation. It is presumed that the replacement of Asn with a smaller Ala produced enough space for a new water molecule to bind to the Nπ of D1-His-190 instead of the Asn C = O. Thus, the hydrogen-bonding pattern of the Y_Z/D1-His-190/D1-Asn-298 triad was probably unchanged in the Y_Z/D1-His-190/H_2O triad in the mutant, although the possibility remains that in intact PSII with the Mn_4CaO_5 cluster, the mutation has some effect on the Y_Z interaction through the hydrogen-bond network around the Mn_4CaO_5 cluster.

The reaction process of the $S_1 \rightarrow S_2$ transition is thought to be simple electron transfer from the Mn_4CaO_5 cluster to $Y_Z^{\bullet}$. Hence, if electron transfer from the Mn_4CaO_5 cluster to $Y_Z^{\bullet}$ is impaired by the D1-N298A mutation, the efficiency of the $S_1 \rightarrow S_2$ transition should also be affected. The S_2/S_1 FTIR difference spectra of WT* and the D1-N298A mutant at the first flash (Figs. 4*A*, *a*, and 5*a*) showed similar overall features but with intensity changes and slight frequency shifts in some bands. At the second flash, the spectrum of D1-N298A showed very similar features to the spectrum of WT* representing the $S_2 \rightarrow S_3$ transition (Figs. 4*A, b,* and 5*b*), although the mutant spectrum had a smaller overall intensity (~60% of WT*). The absence of the features of the S_2/S_1 spectrum in the second-flash spectrum of the mutant (*e.g.* 1432 cm^{-1} peak characteristic of the first-flash spectrum was not involved in the second-flash spectrum) indicates that the $S_1 \rightarrow S_2$ efficiency in D1-N298A is as high as that in WT*. In addition, the peak temperatures of the TL glow curves at 14 and 34 °C arising from charge recombination of $S_2Q_A^-$ (Q band) and $S_2Q_B^-$ (B band), respectively, little changed upon the D1-N298A mutation (Fig. 2*B*). This indicates that the redox potential of the $S_1 \rightarrow S_2$ transition of the Mn_4CaO_5 cluster, which should regulate the electron transfer reaction, is virtually unchanged by this mutation. These observations suggest that the D1-N298A mutation little affected the electron transfer from the Mn_4CaO_5 cluster to $Y_Z^{\bullet}$ at least during the $S_1 \rightarrow S_2$ transition.

In contrast to unaffected electron transfer, the hydrogen-bond network around the Mn_4CaO_5 cluster was clearly affected by the D1-N298A mutation, as revealed by the following observations. (i) The symmetric COO^- region (1450–1300 cm^{-1}) in the S_2/S_1 FTIR difference spectra showed characteristic changes, such as intensity decreases of the 1417 and 1364 cm^{-1} bands by the mutation (Figs. 4*A, a,* and 5*a*). These bands were recently assigned to the symmetric COO^- vibrations of D1-Asp-342/D1-Asp-61 and D1-Asp-170/D1-Glu-333/D1-Asp-342/D1-Glu-189, respectively, by quantum mechanics/molecular mechanics (QM/MM) calculations (85), suggesting slight perturbations of these carboxylate groups by the mutation. (ii) A negative band at 1747 cm^{-1} in the S_2/S_1 spectrum and a positive band at 1745 cm^{-1} in the S_3/S_2 spectrum (Fig. 4*B*), which have been assigned to the CO stretching vibrations of unidentified COOH groups (52, 56), diminished in the spectra of the D1-N298A mutant, indicating the pK_a changes of these COOH groups were located on a common hydrogen-bond network involving D1-Asn-298. (iii) The intensities of the amide II bands in the 1590–1500 cm^{-1} region together with an amide I band at 1652 cm^{-1} in the S_2/S_1 spectrum significantly decreased (Figs. 4*A, a,* and 5*a*), suggesting the perturbation of the backbone interactions near D1-Asn-298. (iv) A negative band at 3662 cm^{-1} in the weakly hydrogen-bonded OH region of water (57, 77, 87) in the S_2/S_1 spectrum diminished and a broader negative band at 3620 cm^{-1} in the S_3/S_2 spectrum (57, 77) seemed slightly downshifted (Fig. 6*A*). (v) The intensity of the feature in the 3000–2600 cm^{-1} region, which have been assigned to strongly hydrogen-bonded OH vibrations of water molecules (77, 87) overlapping the NH vibration of protonated D1-His-337 (88), in the S_2/S_1 difference spectrum decreased by the D1-N298A mutation (Fig. 6*B, a*). In addition, in the similar region in the S_3/S_2 spectrum, a positive band newly appeared at 2907 cm^{-1} (Fig. 6*B, b*). These spectral changes in (iv) and (v)

represent some perturbations in the hydrogen-bonded structure of a water network near the Mn_4CaO_5 cluster by the D1-N298A mutation.

Similar changes in the symmetric COO^-, COOH, and amide II regions in FTIR difference spectra have been previously observed in site-directed mutants of D1-Asp-61, D1-Glu-65, D2-Lys-317, D2-Glu-312, and D1-Arg-334 on the Cl path, and those of D1-Gln-165 near Y_Z and D1-Glu-329 on the Y_Z-O1 path (Fig. 1*A*) (52, 54–57). In addition, the similar decrease in the weakly hydrogen-bonded OH band at ~3662 cm^{-1} and the broad feature in the 3000–2400 cm^{-1} region in the S_2/S_1 difference spectrum was observed in the D1-D61A mutant (57). Indeed, the contribution of W1, which directly interacts with D1-Asp-61, to the bands at ~3662 and 3000–2400 cm^{-1} was suggested by the QM/MM calculation (87). Recently, diminishing of the ~3662 cm^{-1} band in the S_2/S_1 spectrum was also observed in PSII in which Ca^{2+} is substituted with Sr^{2+} (89). All of the above observations, therefore, indicate that a hydrogen-bond network structurally coupled with the Mn_4CaO_5 cluster is widely extended across the channels near Cl and Y_Z involving D1-Asn-298.

The S_3/S_2 FTIR difference spectrum at the second flash decreased its overall intensity to ~60% of WT* by the D1-N298A mutation (Figs. 4*A, b,* and 5*b*). Furthermore, the FTIR spectra at the third and fourth flashes showed very small intensities (Figs. 4*A* and 5). These observations were identical between samples in hydrated films (Fig. 4) and solutions (Fig. 5). These FTIR data of isolated PSII core complexes are consistent with the *in vivo* data of DL measurements using D1-N298A cells, in which the DL intensity monotonically increased with the flash number and reached near maximum by 4 or 5 flashes, in contrast to WT* cells that showed a clear period-four oscillation (Fig. 2*C*). In addition, the 10-fold decrease in the O_2 evolution activity by the D1-N298A mutation was identical between cells and PSII core complexes. These results indicate that the intensity changes in the FTIR spectra by mutation are ascribed to neither the core preparations nor the measurement conditions, but represent the real changes in efficiencies in the S-state transitions. It is thus concluded that the efficiency of the $S_2 \rightarrow S_3$ transition is lowered to ~60% and the $S_3 \rightarrow S_0$ transition is significantly inhibited upon the D1-N298A mutation.

It is generally accepted that one and two protons are released in the $S_2 \rightarrow S_3$ and $S_3 \rightarrow S_0$ transitions, respectively (24–26). With the absence of the prominent effect on the electron transfer from the Mn_4CaO_5 cluster to $Y_Z^{\bullet}$ in the $S_1 \rightarrow S_2$ transition, together with the unlikeliness of direct involvement of D1-Asn-298 in the catalytic reaction at the Mn_4CaO_5 cluster because of its remote distance, the observed efficiency decreases in the $S_2 \rightarrow S_3$ and $S_3 \rightarrow S_0$ transitions suggest that the proton transfer from the catalytic site are partially and significantly inhibited in the $S_2 \rightarrow S_3$ and $S_3 \rightarrow S_0$ transitions, respectively, in the D1-N298A mutant. Alternative possibilities, however, cannot be excluded at the present stage that electron transfer reactions are affected in the S-state transitions other than $S_1 \rightarrow S_2$ and the mutation provides some indirect effect on the catalytic reaction at the Mn_4CaO_5 cluster through a hydrogen-bond network. So far, various mutants at residues near the putative proton/water channels, such as D1-D61A/N/E (46–48, 53, 57, 58), D2-K317R/A/E/Q (54, 55), D1-N181A/S (59), D1-D59N (48), D1-E65A (52), D2-E312A (52), D1-R334A/V/E (49, 56), D1-V185N (58), CP43-R357K (51), D1-Q165E (56), and D1-E329Q (52), have been examined to investigate the effects of mutations on the S-state transitions. However, none of these mutants apparently blocked the $S_2 \rightarrow S_3$ transition. Although some changes in the symmetric COO^- stretching region of the second-flash FTIR spectra in mutants at the D1-Glu-65/D2-Glu-312/D1-Arg-334 triad were interpreted to be due to a decreased $S_2 \rightarrow S_3$ efficiency (52, 56), electrostatic effects by mutations of charged amino acid residues have not been identified. In addition, although the D1-D61N mutation slowed the $S_2 \rightarrow S_3$ transition by a factor of 2–4, the $S_1 \rightarrow S_2$ transition was also slowed by a similar extent, and hence this retardation was suggested to be caused by the increase in the redox potential of the Mn_4CaO_5 cluster (47, 53). The partial inhibition of the $S_2 \rightarrow S_3$ efficiency in the D1-N298A mutant observed in our study suggests that when the main proton pathway was blocked by this mutation, another pathway was used for the proton exit in the $S_2 \rightarrow S_3$ transition or this transition originally uses multiple proton pathways. Such flexible proton transfer through different pathways may be realized by a widely extended hydrogen-bond network involving several different pathways around the Mn_4CaO_5 cluster mentioned above.

Because significant inhibition by the D1-N298A mutation was observed in the $S_3 \rightarrow S_0$ transition, at least one of two protons released in this transition most likely uses the pathway near Y_Z perturbed by this mutation. The other proton may use the Cl path because mutations at D1-Asp-61, D2-Lys-317, D1-Asn-181, and the D1-Glu-65/D2-Glu-312/D1-Arg-334 triad substantially lowered the efficiency of this transition or significantly retarded the O_2 evolution kinetics.

A tight hydrogen-bond network is advantageous to rapid proton transfer using the Grotthuss mechanism rather than a network of mobile water molecules. Previous MD simulation by Ogata *et al.* (36) showed that water molecules in the Y_Z-Asn-298 path ("path 1" in Ref. 36) showed only small fluctuations. In addition, Sakashita *et al.* (39) recently showed by MD simulation of water accessibility that water molecules near D1-Asn-298 are less exchangeable in contrast to exchangeable water molecules in the Y_Z-O1 path and the Cl path ("O1-water chain" and "Glu-65/Glu-312 channel," respectively, in Ref. 39), and suggested the involvement of the hydrogen-bond network near D1-Asn-298 in proton transfer. In the D1-N298A mutant, the tight hydrogen-bond network near D1-Asn-298 should be disrupted and may be replaced by a loose water network, which would retard the proton transfer from the catalytic site. Although this mutation may also loosen the structure of a water cluster near O1 in the Y_Z-O1 path, the effect would be minor because water molecules in this channel are originally mobile as shown in previous MD simulations (33, 35, 36, 39). In contrast to proton transfer, channels involving mobile water molecules are advantageous to water transfer. Although insertion of substrate water to the catalytic site has been suggested to occur in the $S_2 \rightarrow S_3$ and $S_3 \rightarrow S_0$ transitions (40, 42, 43, 66, 76, 90–93), the loosened water network possibly produced by the D1-N298A mutation would not inhibit water insertion. Thus, the N298A-induced inhibition of the $S_2 \rightarrow S_3$ and $S_3 \rightarrow S_0$ tran-

sitions observed in the present study is more likely caused by the impairment of proton transfer rather than water transfer. One possible mechanism of proton transfer through the Y_Z site has been proposed from FTIR and QM/MM analyses (16, 70). QM/MM calculations showed that upon Y_Z oxidation, the network of nearby water molecules is rearranged and one water molecule moves toward D1-His-190. The proton that was shifted from Y_Z to the Nτ of D1-His-190 has a large polarizability as revealed by a broad feature at ~2800 cm^{-1} in a $Y_Z^{\bullet}/Y_Z$ FTIR spectrum (16). It was thus proposed that this proton between $Y_Z^{\bullet}$ and $HisH^+$ may have a chance to hop to the nearby water, probably using NH bending vibration, followed by immediate proton transfer through a water chain supported by D1-Asn-298. An alternative proposal was proton transfer from W4, a ligand to Ca^{2+}, or a nearby water to the water chain near D1-Asn-298. The transferred proton from D1-His-190 or W4 will be immediately replenished by a proton from a substrate water through a water network between Y_Z and Mn4 (Fig. 1*A*) using coupled OH stretching vibrations extended to several water molecules (87). Note that this proton transfer mechanism is different from the previous so-called hydrogen abstraction model (94), in which the proton of Y_Z is first released to the bulk upon its oxidization. The driving force of the above proton transfer process is charge repulsion between the protonated cation of D1-His-190 and the excess positive charge on the Mn_4CaO_5 cluster in the S_2 and S_3 states. Also, proton release needs to take place before electron transfer in the $S_2 \rightarrow S_3$ and $S_3 \rightarrow S_0$ transitions to decrease the redox potential of the Mn_4CaO_5 cluster (42). Thus, this proton transfer mechanism through the Y_Z site can be functional in the $S_2 \rightarrow S_3$ transition and for the first proton in the $S_3 \rightarrow S_0$ transition. Indeed, proton transfer as a lag phase (~30 μs) before electron transfer (42) or as a rate-limiting step (~350 μs) coupled to electron transfer (43) have been proposed in the $S_2 \rightarrow S_3$ transition, whereas a lag phase (~200 μs) before the electron transfer/O_2 evolution phase in the $S_3 \rightarrow S_0$ transfer has been attributed to a proton transfer process (58, 95–97). These putative proton transfer processes during the $S_2 \rightarrow S_3$ and $S_3 \rightarrow S_0$ transitions take place in the similar time regime of tens or hundreds of microseconds (42, 43, 58, 95–97), suggesting that they are performed by a similar proton transfer mechanism. However, the extent of inhibition by the D1-Asn-298 mutation was different between these transitions: the $S_2 \rightarrow S_3$ transition is only partially inhibited, whereas the $S_3 \rightarrow S_0$ transition is more significantly blocked. This difference could be related to different hydrogen-bonded structures around the Mn_4CaO_5 cluster between the S_2- and S_3-states and their changes upon mutation, which are revealed by a broad positive feature in the strongly hydrogen-bonded OH region at 2800–2400 cm^{-1} in the S_3/S_2 FTIR difference spectrum (57, 77) and a change in the mutant such as the appearance of a positive feature at 2907 cm^{-1} (Fig. 6*B, b*).

In conclusion, spectroscopic analyses of the D1-N298A mutant suggest that the hydrogen-bond network near Y_Z is functional in proton transfer during water oxidation, especially in the $S_2 \rightarrow S_3$ and $S_3 \rightarrow S_0$ transitions. D1-Asn-298 plays a pivotal role in forming a tight hydrogen-bond network near Y_Z, which is crucial for efficient proton transfer. At the present stage, however, possibilities other than proton transfer as an inhibited process by the mutation cannot be fully excluded. Further studies using this mutant as well as other site-directed mutants of residues on putative proton pathways, in combination with spectroscopic analyses such as time-resolved infrared spectroscopy, are necessary for identifying proton release pathways for four individual protons in the S-state cycle. Such studies of proton transfer are crucial for full understanding of the mechanism of photosynthetic water oxidation.

Experimental procedures

Construction of site-directed mutant

The wild-type control strain of the D1 subunit (WT*) and the D1-N298A strain were constructed in *Synechocystis* sp. PCC 6803 with an analogous method of Nagao *et al.* (71). Plasmid pRN123, which involved the coding region of *psbA2*, was used as a parental vector for site-directed mutagenesis. A host *Synechocystis* strain, which was transformed with pRN123 to obtain the WT* strain, lacked all of the three *psbA* genes (Δ*psbA1*/Δ*psbA2*/Δ*psbA3*) and contains a His_6 tag attached to the C terminus of CP47 (71). Mutation of D1-Asn-298 to Ala was introduced into pRN123 by replacing an AAC codon at a target site with a GCC codon, and the resultant plasmid was introduced into the host Δ*psbA1*/Δ*psbA2*/Δ*psbA3* strain.

The WT* and D1-N298A strains were maintained on BG-11 (98) agar plates containing 5 μg ml^{-1} of kanamycin (Km), 5 μg ml^{-1} of chloramphenicol (Cm), 5 μg ml^{-1} of erythromycin (Em), and 5 μg ml^{-1} of spectinomycin (Sm) in the presence of 5 mM glucose and 10 μM 3-(3,4)-dichlorophenyl-1,1-dimethylurea (DCMU) under a continuous low-light condition. The genotype of the D1-N298A mutant was confirmed by PCR analysis and DNA sequencing in both cases of *in vivo* analyses and preparation of PSII core complexes for FTIR measurements. No trace of the wild-type *psbA2* gene was detected in any cultures of the D1-N298A strain.

Cell growth

WT* and D1-N298A cells were grown photoautotrophically in 40 ml of a BG-11 medium (98) supplemented with 4 mM Hepes-NaOH (pH 7.5) and 5 μg ml^{-1} Km/Cm/Em/Sm by bubbling with air containing 1% (v/v) CO_2 at 30 °C under continuous illumination (20 μmol of photons m^{-2} s^{-1}) by white fluorescence lamps. The cell density was monitored as an optical density at 730 nm (A_{730}) using a spectrophotometer (Shimadzu UV-3100PC). For *in vivo* analyses, cells grown to the concentration of A_{730} = 0.5–1.0 were inoculated into 40 ml of a fresh BG-11 medium without antibiotics (A_{730} = ~0.1), and were cultured under the same condition. Log-phase cells were collected by centrifugation (1000 × *g* for 5 min at 25 °C) and suspended in a BG-11 medium. For PSII preparation, cells were grown in an 8-liter culture bottle without antibiotics under the photoautotrophic growth condition. Cells cultured in six bottles (total volume of 48 liters) were used for preparation of PSII core complexes from each strain.

Preparation of PSII core complexes

O_2-evolving PSII core complexes were purified using the method by Nagao *et al.* (71) with a minor modification. Thyla-

koid membranes suspended in a buffer (pH 6.0) containing 50 mM Mes-NaOH, 5 mM $CaCl_2$, 10 mM $MgCl_2$, and 25% (w/v) glycerol (buffer A) were solubilized with 1% (w/v) *n*-dodecyl β-D-maltoside (DM) at a Chl concentration of 1.0 mg ml^{-1} by stirring for 10 min on ice. After centrifugation at 27,000 × *g* for 15 min, the resultant supernatant was applied to a Ni^{2+} affinity column equilibrated with buffer A containing 0.04% DM (buffer B). The column was washed with 1 volume of buffer B containing 5 mM L-histidine followed by further washing with buffer B. PSII complexes were eluted with buffer B containing 50 mM L-histidine and then concentrated by ultrafiltration (Vivaspin 20, 100 kDa MWCO, Sartorius Stedim). The isolated PSII complexes were stored in liquid nitrogen.

Measurement of O_2 evolution activity

The O_2 evolution activity was measured using a Clark-type oxygen electrode at 30 °C under a saturating light condition. The activities of cell samples (10 μg of Chl) were measured in BG-11 medium in the presence of 1 mM DCBQ and 1 mM potassium ferricyanide as electron acceptors, whereas those of PSII complexes (3.5–5 μg of Chl) were measured in a buffer (pH 6.0) containing 1 M sucrose, 5 mM $CaCl_2$, 10 mM NaCl, and 50 mM Mes-NaOH in the presence of 0.1 mM DCBQ and 4 mM potassium ferricyanide as electron acceptors.

TL and DL measurements

TL and DL were measured using a laboratory-built apparatus, as described previously (99). Before measurements, cells suspended in BG-11 medium (250 μg of Chl ml^{-1}) were exposed to white continuous light (200 μmol of photons m^{-2} s^{-1}; ~16 milliwatt cm^{-2} at the sample point) for 30 s at 30 °C, followed by incubation at this temperature for 5 min in the dark. A cell suspension (70 μl) was then loaded onto a piece of filter paper. For detection of a TL B band ($S_2Q_B^-$ recombination), the sample was illuminated by a single saturating flash from a Xe lamp (SL-230S, Sugawara) at 5 °C, whereas for a TL Q band ($S_2Q_A^-$ recombination), the sample in the presence of 50 μM DCMU was illuminated with continuous white light (~55 milliwatt cm^{-2} at the sample point) from a halogen lamp (MEJIRO PRECISION PHL-150) for 10 s at −20 °C. The illuminated sample was quickly cooled down and then warmed at a rate of 40 °C min^{-1} to record a TL glow curve.

For DL measurement, the sample was illuminated by a series of saturating Xe flashes (1 Hz) at 25 °C, and DL emission upon each flash was recorded. The DL amplitude at 0.8 s after each flash was plotted against a flush number. The measurement was performed once for each sample, and the data obtained using three different samples were averaged.

FTIR measurements

Light-induced FTIR difference spectra were recorded using a Bruker IFS-66/S spectrophotometer equipped with an MCT detector (InfraRed D313-L) at 4 cm^{-1} resolution. Flash illumination was performed by a Q-switched Nd:YAG laser (Quanta-Ray GCR-130; 532 nm, ~7 ns full width at half-maximum) with a power of ~7 mJ $pulse^{-1}$ cm^{-2} at a sample point.

FTIR measurements of the S-state transitions in PSII core complexes were performed following the previous methods (26, 74, 76, 77). PSII complexes were washed with a buffer (pH 6.0) containing 10 mM Mes-NaOH, 5 mM NaCl, 5 mM $CaCl_2$, 40 mM sucrose, and 0.06% DM (buffer C) and concentrated to ~2.5 mg of Chl ml^{-1} by ultrafiltration (Apollo 7-ml High-Performance Centrifugal Concentrators, 150 kDa MWCO, Orbital Biosciences). Two sample types, solutions and moderately hydrated films, were used for measurements. For solution samples, 10 μl of the PSII solution (~2.5 mg of Chl ml^{-1}) in buffer C mixed with 1 μl of 100 mM potassium ferricyanide (total volume: 11 μl) was lightly dried on a CaF_2 plate (25 mm in diameter) under N_2 gas flow. The resultant sample was then mixed with 1 μl of Milli-Q water, and sandwiched with another CaF_2 plate with a circular groove (14-mm inner diameter; 1-mm width). The sample cell was sealed with silicone grease in the outer part of the groove, where a tiny piece of aluminum foil was placed as a spacer. For preparation of a hydrated film, 4.5 μl of PSII solution (~2.5 mg of Chl ml^{-1}) in buffer C mixed with additional 5.5 μl of buffer C and 1 μl of 100 mM potassium ferricyanide (total volume: 11 μl) was dried on a CaF_2 plate (25 × 25 mm) in a circle shape (8 mm in diameter) under N_2 gas flow. The resultant sample was sealed using another CaF_2 plate and a silicone spacer (0.5 mm in thickness), enclosing 2 μl of 40% (v/v) glycerol solution (95% relative humidity) without touching the sample to moderately hydrate the film (76). For both types of samples, the sample temperature was kept at 10 °C by circulating cold water through a copper holder.

In the measurement of a moderately hydrated film, two preflashes with a 1-s interval were first applied to the sample followed by dark adaptation for 15 min to synchronize all centers to the S_1 state. Four flashes were then applied with intervals of 10 s; a single-beam spectrum with 20 scans (10-s scan) was measured twice before the first flash and once after individual flashes. The whole measurement scheme was repeated 12 times, and the spectra were averaged using five different samples (total 1200 scans). The measurement of a solution sample was performed using the same scheme, but with the dark interval of 10 min. The measurement was repeated 24 times using one sample, and the spectra were averaged (total 480 scans). To obtain better signal-to-noise ratios in the 3700–2200 cm^{-1} region of the spectra in the $S_1 \rightarrow S_2$ and $S_2 \rightarrow S_3$ transitions, measurements by two flashes were performed using the hydrated films. In this case, preflashes except for the first ones were omitted because the S_2- and S_3-states returned back to the S_1-state during dark adaptation for 15 min. Other conditions were the same as the four-flash measurements of the hydrated films. The measurement was repeated 120 times, and the spectra using four samples were averaged (total 8400 scans). These average spectra were used to calculate flash-induced spectra of the S-state transitions together with a dark-minus-dark spectrum representing a noise level.

$Y_Z^{\bullet}/Y_Z$ FTIR difference spectra were measured following the method described previously (16) with a slight modification. Mn depletion was performed by 10 mM NH_2OH treatment for 1 h on ice, followed by washing four times with a buffer (pH 6.5) containing 20 mM Mes-NaOH, 5 mM NaCl, and 0.06% DM using ultrafiltration (Vivaspin 500, 100 kDa MWCO, Sartorius Stedim), which finally concentrated the sample to 2.5 mg of Chl ml^{-1}. An aliquot (8 μl) of the sample solution, which was mixed

with 1 μl of 100 mM potassium ferricyanide, was dried on a BaF_2 plate (13 mm in diameter) under a N_2 gas flow, and then sandwiched with another BaF_2 plate together with 0.85 μl of Milli-Q water. The sample temperature was adjusted to 250 K in a cryostat (Oxford DN1704). Single-beam spectra with 50 scans (25-s scan) were recorded twice before and once after a single flash. This measurement was repeated 90 and 160 times for WT* and D1-N298A, respectively, with a dark interval of 225 s, and the average spectra were used to calculate a $Y_Z^{\bullet}/Y_Z$ spectrum together with a dark-minus-dark spectrum representing a noise level.

Author contributions—R. N. and T. N. designed the study and wrote the manuscript. R. N. and H. U.-N. performed the experiments. All authors reviewed the results and approved the final version of the manuscript.

References

1. Blankenship, R. E. (2002) *Molecular Mechanisms of Photosynthesis*, Blackwell Science, Oxford, UK
2. Debus, R. J. (1992) The manganese and calcium ions of photosynthetic oxygen evolution. *Biochim. Biophys. Acta* **1102,** 269–352
3. McEvoy, J. P., and Brudvig, G. W. (2006) Water-splitting chemistry of photosystem II. *Chem. Rev.* **106,** 4455–4483
4. Dau, H., and Haumann, M. (2008) The manganese complex of photosystem II in its reaction cycle: basic framework and possible realization at the atomic level. *Coord. Chem. Rev.* **252,** 273–295
5. Renger, G. (2012) Mechanism of light induced water splitting in Photosystem II of oxygen evolving photosynthetic organisms. *Biochim. Biophys. Acta* **1817,** 1164–1176
6. Messinger, J., Noguchi, T., and Yano, J. (2012) in *Molecular Solar Fuels* (Wydrzynski, T. J., and Hillier, W., eds) pp. 163–207, Royal Society of Chemistry, Cambridge, UK
7. Cox, N., and Messinger, J. (2013) Reflections on substrate water and dioxygen formation. *Biochim. Biophys. Acta* **1827,** 1020–1030
8. Yano, J., and Yachandra, V. (2014) Mn_4Ca cluster in photosynthesis: where and how water is oxidized to dioxygen. *Chem. Rev.* **114,** 4175–4205
9. Shen, J.-R. (2015) The structure of photosystem II and the mechanism of water oxidation in photosynthesis. *Annu. Rev. Plant Biol.* **66,** 23–48
10. Diner, B. A., and Rappaport, F. (2002) Structure, dynamics, and energetics of the primary photochemistry of photosystem II of oxygenic photosynthesis. *Annu. Rev. Plant Biol.* **53,** 551–580
11. Renger, G., and Holzwarth, A. R. (2005) in *Photosystem II: The Light-Driven Water:Plastoquinone Oxidoreductase* (Wydrzynski, T. J., and Satoh, K., eds) pp. 139–175, Springer, Dordrecht, The Netherlands
12. Petrouleas, V., and Crofts, A. R. (2005) in *Photosystem II: The Light-Driven Water:Plastoquinone Oxidoreductase* (Wydrzynski, T. J., and Satoh, K., eds) pp. 177–206, Springer, Dordrecht, The Netherlands
13. Diner, B. A., and Britt, R. D. (2005) in *Photosystem II: The Light-Driven Water:Plastoquinone Oxidoreductase* (Wydrzynski, T. J., and Satoh, K., eds) pp. 207–233, Springer, Dordrecht, The Netherlands
14. Styring, S., Sjöholm, J., and Mamedov, F. (2012) Two tyrosines that changed the world: Interfacing the oxidizing power of photochemistry to water splitting in photosystem II. *Biochim. Biophys. Acta* **1817,** 76–87
15. Saito, K., Shen, J.-R., Ishida, T., and Ishikita, H. (2011) Short hydrogen bond between redox-active tyrosine Y_Z and D1-His190 in the photosystem II crystal structure. *Biochemistry* **50,** 9836–9844
16. Nakamura, S., Nagao, R., Takahashi, R., and Noguchi, T. (2014) Fourier transform infrared detection of a polarizable proton trapped between photooxidized tyrosine Y_Z and a coupled histidine in photosystem II: relevance to the proton transfer mechanism of water oxidation. *Biochemistry* **53,** 3131–3144
17. Umena, Y., Kawakami, K., Shen, J.-R., and Kamiya, N. (2011) Crystal structure of oxygen-evolving photosystem II at a resolution of 1.9 Å. *Nature* **473,** 55–60
18. Suga, M., Akita, F., Hirata, K., Ueno, G., Murakami, H., Nakajima, Y., Shimizu, T., Yamashita, K., Yamamoto, M., Ago, H., and Shen, J.-R. (2015) Native structure of photosystem II at 1.95-Å resolution viewed by femtosecond X-ray pulses. *Nature* **517,** 99–103
19. Young, I. D., Ibrahim, M., Chatterjee, R., Gul, S., Fuller, F. D., Koroidov, S., Brewster, A. S., Tran, R., Alonso-Mori, R., Kroll, T., Michels-Clark, T., Laksmono, H., Sierra, R. G., Stan, C. A., Hussein, R., *et al.* (2016) Structure of photosystem II and substrate binding at room temperature. *Nature* **540,** 453–457
20. Tanaka, A., Fukushima, Y., and Kamiya, N. (2017) Two different structures of the oxygen-evolving complex in the same polypeptide frameworks of photosystem II. *J. Am. Chem. Soc.* **139,** 1718–1721
21. Suga, M., Akita, F., Sugahara, M., Kubo, M., Nakajima, Y., Nakane, T., Yamashita, K., Umena, Y., Nakabayashi, M., Yamane, T., Nakano, T., Suzuki, M., Masuda, T., Inoue, S., Kimura, T., *et al.* (2017) Light-induced structural changes and the site of O=O bond formation in PSII caught by XFEL. *Nature* **543,** 131–135
22. Joliot, P., Barbieri, G., and Chabaud, R. (1969) A new model of the photochemical centers in system II. *Photochem. Photobiol.* **10,** 309–329
23. Kok, B., Forbush, B., and McGloin, M. (1970) Cooperation of charges in photosynthetic O_2 evolution: I. a linear four step mechanism. *Photochem. Photobiol.* **11,** 457–475
24. Förster, V., and Junge, W. (1985) Stoichiometry and kinetics of proton release upon photosynthetic water oxidation. *Photochem. Photobiol.* **41,** 183–190
25. Schlodder, E., and Witt, H. T. (1999) Stoichiometry of proton release from the catalytic center in photosynthetic water oxidation: reexamination by a glass electrode study at pH 5.5–7.2. *J. Biol. Chem.* **274,** 30387–30392
26. Suzuki, H., Sugiura, M., and Noguchi, T. (2009) Monitoring proton release during photosynthetic water oxidation in photosystem II by means of isotope-edited infrared spectroscopy. *J. Am. Chem. Soc.* **131,** 7849–7857
27. Ferreira, K. N., Iverson, T. M., Maghlaoui, K., Barber, J., and Iwata, S. (2004) Architecture of the photosynthetic oxygen-evolving center. *Science* **303,** 1831–1838
28. Guskov, A., Kern, J., Gabdulkhakov, A., Broser, M., Zouni, A., and Saenger, W. (2009) Cyanobacterial photosystem II at 2.9-Å resolution and the role of quinones, lipids, channels and chloride. *Nat. Struct. Mol. Biol.* **16,** 334–342
29. Ishikita, H., Saenger, W., Loll, B., Biesiadka, J., and Knapp, E.-W. (2006) Energetics of a possible proton exit pathway for water oxidation in photosystem II. *Biochemistry* **45,** 2063–2071
30. Murray, J. W., and Barber, J. (2007) Structural characteristics of channels and pathways in photosystem II including the identification of an oxygen channel. *J. Struct. Biol.* **159,** 228–237
31. Ho, F. M., and Styring, S. (2008) Access channels and methanol binding site to the $CaMn_4$ cluster in Photosystem II based on solvent accessibility simulations, with implications for substrate water access. *Biochim. Biophys. Acta* **1777,** 140–153
32. Gabdulkhakov, A., Guskov, A., Broser, M., Kern, J., Müh, F., Saenger, W., and Zouni, A. (2009) Probing the accessibility of the Mn_4Ca cluster in photosystem II: channels calculation, noble gas derivatization, and cocrystallization with DMSO. *Structure* **17,** 1223–1234
33. Vassiliev, S., Comte, P., Mahboob, A., and Bruce, D. (2010) Tracking the flow of water through photosystem II using molecular dynamics and streamline tracing. *Biochemistry* **49,** 1873–1881
34. Rivalta, I., Amin, M., Luber, S., Vassiliev, S., Pokhrel, R., Umena, Y., Kawakami, K., Shen, J.-R., Kamiya, N., Bruce, D., Brudvig, G. W., Gunner, M. R., and Batista, V. S. (2011) Structural-functional role of chloride in photosystem II. *Biochemistry* **50,** 6312–6315
35. Vassiliev, S., Zaraiskaya, T., and Bruce, D. (2012) Exploring the energetics of water permeation in photosystem II by multiple steered molecular dynamics simulations. *Biochim. Biophys. Acta* **1817,** 1671–1678
36. Ogata, K., Yuki, T., Hatakeyama, M., Uchida, W., and Nakamura, S. (2013) All-atom molecular dynamics simulation of photosystem II embedded in thylakoid membrane. *J. Am. Chem. Soc.* **135,** 15670–15673

37. Linke, K., and Ho, F. M. (2014) Water in Photosystem II: Structural, functional and mechanistic considerations. *Biochim. Biophys. Acta* **1837,** 14–32
38. Saito, K., Rutherford, A. W., and Ishikita, H. (2015) Energetics of proton release on the first oxidation step in the water-oxidizing enzyme. *Nat. Commun.* **6,** 8488
39. Sakashita, N., Watanabe, H. C., Ikeda, T., Saito, K., and Ishikita, H. (2017) Origins of water molecules in the photosystem II crystal structure. *Biochemistry* **56,** 3049–3057
40. Siegbahn, P. E. (2012) Mechanisms for proton release during water oxidation in the S_2 to S_3 and S_3 to S_4 transitions in photosystem II. *Phys. Chem. Chem. Phys.* **14,** 4849–4856
41. Amin, M., Vogt, L., Szejgis, W., Vassiliev, S., Brudvig, G. W., Bruce, D., and Gunner, M. R. (2015) Proton-coupled electron transfer during the S-state transitions of the oxygen-evolving complex of photosystem II. *J. Phys. Chem. B* **119,** 7366–7377
42. Klauss, A., Haumann, M., and Dau, H. (2012) Alternating electron and proton transfer steps in photosynthetic water oxidation. *Proc. Natl. Acad. Sci. U.S.A.* **109,** 16035–16040
43. Sakamoto, H., Shimizu, T., Nagao, R., and Noguchi, T. (2017) Monitoring the reaction process during the $S_2 \rightarrow S_3$ transition in photosynthetic water oxidation using time-resolve infrared spectroscopy. *J. Am. Chem. Soc.* **139,** 2022–2029
44. Wei, X., Su, X., Cao, P., Liu, X., Chang, W., Li, M., Zhang, X., and Liu, Z. (2016) Structure of spinach photosystem II-LHCII supercomplex at 3.2-Å resolution. *Nature* **534,** 69–74
45. Su, X., Ma, J., Wei, X., Cao, P., Zhu, D., Chang, W., Liu, Z., Zhang, X., and Li, M. (2017) Structure and assembly mechanism of plant $C_2S_2M_2$-type PSII-LHCII supercomplex. *Science* **357,** 815–820
46. Chu, H.-A., Nguyen, A. P., and Debus, R. J. (1995) Amino acid residues that influence the binding of manganese or calcium to photosystem II: 1. the lumenal interhelical domains of the D1 polypeptide. *Biochemistry* **34,** 5839–5858
47. Hundelt, M., Hays, A.-M., Debus, R. J., and Junge, W. (1998) Oxygenic photosystem II: the mutation D1-D61N in *Synechocystis* sp. PCC 6803 retards S-state transitions without affecting electron transfer from Y_Z to $P680^+$. *Biochemistry* **37,** 14450–14456
48. Qian, M., Dao, L., Debus, R. J., and Burnap, R. L. (1999) Impact of mutations within the putative Ca^{2+}-binding lumenal interhelical a-b loop of the photosystem II D1 protein on the kinetics of photoactivation and H_2O-oxidation in *Synechocystis* sp PCC6803. *Biochemistry* **38,** 6070–6081
49. Li, Z., and Burnap, R. L. (2002) Mutations of basic arginine residue 334 in the D1 protein of Photosystem II lead to unusual S_2 state properties in *Synechocystis* sp. PCC 6803. *Photosynth. Res.* **72,** 191–201
50. Yamasato, A., Kamada, T., and Satoh, K. (2002) Random mutagenesis targeted to the *psbA*II gene of *Synechocystis* sp. PCC 6803 to identify functionally important residues in the D1 protein of the photosystem II reaction center. *Plant Cell Physiol.* **43,** 540–548
51. Hwang, H. J., Dilbeck, P., Debus, R. J., and Burnap, R. L. (2007) Mutation of arginine 357 of the CP43 protein of photosystem II severely impairs the catalytic S-state cycle of the H_2O oxidation complex. *Biochemistry* **46,** 11987–11997
52. Service, R. J., Hillier, W., and Debus, R. J. (2010) Evidence from FTIR difference spectroscopy of an extensive network of hydrogen bonds near the oxygen-evolving Mn_4Ca cluster of photosystem II involving D1-Glu65, D2-Glu312, and D1-Glu329. *Biochemistry* **49,** 6655–6669
53. Dilbeck, P. L., Hwang, H. J., Zaharieva, I., Gerencser, L., Dau, H., and Burnap, R. L. (2012) The D1-D61N mutation in *Synechocystis* sp. PCC 6803 allows the observation of pH-sensitive intermediates in the formation and release of O_2 from photosystem II. *Biochemistry* **51,** 1079–1091
54. Pokhrel, R., Service, R. J., Debus, R. J., and Brudvig, G. W. (2013) Mutation of lysine 317 in the D2 subunit of photosystem II alters chloride binding and proton transport. *Biochemistry* **52,** 4758–4773
55. Suzuki, H., Yu, J., Kobayashi, T., Nakanishi, H., Nixon, P. J., and Noguchi, T. (2013) Functional roles of D2-Lys317 and the interacting chloride ion in the water oxidation reaction of photosystem II as revealed by Fourier transform infrared analysis. *Biochemistry* **52,** 4748–4757
56. Service, R. J., Hillier, W., and Debus, R. J. (2014) Network of hydrogen bonds near the oxygen-evolving Mn_4CaO_5 cluster of photosystem II probed with FTIR difference spectroscopy. *Biochemistry* **53,** 1001–1017
57. Debus, R. J. (2014) Evidence from FTIR difference spectroscopy that D1-Asp61 influences the water reactions of the oxygen-evolving Mn_4CaO_5 cluster of photosystem II. *Biochemistry* **53,** 2941–2955
58. Bao, H., and Burnap, R. L. (2015) Structural rearrangements preceding dioxygen formation by the water oxidation complex of photosystem II. *Proc. Natl. Acad. Sci. U.S.A.* **112,** E6139–E6147
59. Pokhrel, R., Debus, R. J., and Brudvig, G. W. (2015) Probing the effect of mutations of asparagine 181 in the D1 subunit of photosystem II. *Biochemistry* **54,** 1663–1672
60. Kuroda, H., Kodama, N., Sun, X.-Y., Ozawa, S., and Takahashi, Y. (2014) Requirement for Asn298 on D1 protein for oxygen evolution: Analyses by exhaustive amino acid substitution in the green alga *Chlamydomonas reinhardtii*. *Plant Cell Physiol.* **55,** 1266–1275
61. Chu, H.-A., Hillier, W., Law, N. A., and Babcock, G. T. (2001) Vibrational spectroscopy of the oxygen-evolving complex and of manganese model compounds. *Biochim. Biophys. Acta* **1503,** 69–82
62. Noguchi, T., and Berthomieu, C. (2005) in *Photosystem II: The Light-Driven Water:Plastoquinone Oxidoreductase* (Wydrzynski, T. J., and Satoh, K., eds) pp. 367–387, Springer, Dordrecht, The Netherlands
63. Noguchi, T. (2007) Light-induced FTIR difference spectroscopy as a powerful tool toward understanding the molecular mechanism of photosynthetic oxygen evolution. *Photosynth. Res.* **91,** 59–69
64. Debus, R. J. (2008) Protein ligation of the photosynthetic oxygen-evolving center. *Coord. Chem. Rev.* **252,** 244–258
65. Noguchi, T. (2008) Fourier transform infrared analysis of the photosynthetic oxygen-evolving center. *Coord. Chem. Rev.* **252,** 336–346
66. Noguchi, T. (2008) FTIR detection of water reactions in the oxygen-evolving center of photosystem II. *Phil. Trans. R. Soc. B* **363,** 1189–1195
67. Chu, H.-A. (2013) Fourier transform infrared difference spectroscopy for studying the molecular mechanism of photosynthetic water oxidation. *Front. Plant Sci.* **4,** 146
68. Noguchi, T. (2013) Monitoring the reactions of photosynthetic water oxidation using infrared spectroscopy. *Biomed. Spectrosc. Imaging* **2,** 115–128
69. Debus, R. J. (2015) FTIR studies of metal ligands, networks of hydrogen bonds, and water molecules near the active site Mn_4CaO_5 cluster in Photosystem II. *Biochim. Biophys. Acta* **1847,** 19–34
70. Noguchi, T. (2015) Fourier transform infrared difference and time-resolved infrared detection of the electron and proton transfer dynamics in photosynthetic water oxidation. *Biochim. Biophys. Acta* **1847,** 35–45
71. Nagao, R., Yamaguchi, M., Nakamura, S., Ueoka-Nakanishi, H., and Noguchi, T. (2017) Genetically introduced hydrogen bond interactions reveal an asymmetric charge distribution on the radical cation of the special-pair chlorophyll P680. *J. Biol. Chem.* **292,** 7474–7486
72. Vass, I., and Govindjee. (1996) Thermoluminescence from the photosynthetic apparatus. *Photosynth. Res.* **48,** 117–126
73. Berthomieu, C., Hienerwadel, R., Boussac, A., Breton, J., and Diner, B. A. (1998) Hydrogen bonding of redox-active tyrosine Z of photosystem II probed by FTIR difference spectroscopy. *Biochemistry* **37,** 10547–10554
74. Noguchi, T., and Sugiura, M. (2001) Flash-induced Fourier transform infrared detection of the structural changes during the S-state cycle of the oxygen-evolving complex in photosystem II. *Biochemistry* **40,** 1497–1502
75. Hillier, W., and Babcock, G. T. (2001) S-state dependent Fourier transform infrared difference spectra for the photosystem II oxygen evolving complex. *Biochemistry* **40,** 1503–1509
76. Noguchi, T., and Sugiura, M. (2002) Flash-induced FTIR difference spectra of the water oxidizing complex in moderately hydrated photosystem II core films: effect of hydration extent on S-state transitions. *Biochemistry* **41,** 2322–2330
77. Noguchi, T., and Sugiura, M. (2002) FTIR detection of water reactions during the flash-induced S-state cycle of the photosynthetic water-oxidizing complex. *Biochemistry* **41,** 15706–15712
78. Noguchi, T., and Sugiura, M. (2003) Analysis of flash-induced FTIR difference spectra of the S-state cycle in the photosynthetic water-oxidizing complex by uniform ^{15}N and ^{13}C isotope labeling. *Biochemistry* **42,** 6035–6042

79. Kimura, Y., Mizusawa, N., Ishii, A., and Ono, T. (2005) FTIR detection of structural changes in a histidine ligand during S-state cycling of photosynthetic oxygen-evolving complex. *Biochemistry* **44,** 16072–16078
80. Shimada, Y., Suzuki, H., Tsuchiya, T., Tomo, T., Noguchi, T., and Mimuro, M. (2009) Effect of a single-amino acid substitution of the 43 kDa chlorophyll protein on the oxygen-evolving reaction of the cyanobacterium *Synechocystis* sp. PCC 6803: analysis of the Glu354Gln mutation. *Biochemistry* **48,** 6095–6103
81. Service, R. J., Yano, J., McConnell, I., Hwang, H. J., Niks, D., Hille, R., Wydrzynski, T., Burnap, R. L., Hillier, W., and Debus, R. J. (2011) Participation of glutamate-354 of the CP43 polypeptide in the ligation of manganese and the binding of substrate water in photosystem II. *Biochemistry* **50,** 63–81
82. Kimura, Y., Mizusawa, N., Ishii, A., Yamanari, T., and Ono, T. (2003) Changes of low-frequency vibrational modes induced by universal ^{15}N- and ^{13}C-isotope labeling in S_2/S_1 FTIR difference spectrum of oxygen-evolving complex. *Biochemistry* **42,** 13170–13177
83. Noguchi, T., Ono, T., and Inoue, Y. (1995) Direct detection of a carboxylate bridge between Mn and Ca^{2+} in the photosynthetic oxygen-evolving center by means of Fourier transform infrared spectroscopy. *Biochim. Biophys. Acta* **1228,** 189–200
84. Chu, H.-A., Hillier, W., and Debus, R. J. (2004) Evidence that the C-terminus of the D1 polypeptide of photosystem II is ligated to the manganese ion that undergoes oxidation during the S_1 to S_2 transition: an isotope-edited FTIR study. *Biochemistry* **43,** 3152–3166
85. Nakamura, S., and Noguchi, T. (2016) Quantum mechanics/molecular mechanics simulation of the ligand vibrations of the water-oxidizing Mn_4CaO_5 cluster in photosystem II. *Proc. Natl. Acad. Sci. U.S.A.* **113,** 12727–12732
86. Noguchi, T., and Sugiura, M. (2000) Structure of an active water molecule in the water-oxidizing complex of photosystem II as studied by FTIR spectroscopy. *Biochemistry* **39,** 10943–10949
87. Nakamura, S., Ota, K., Shibuya, Y., and Noguchi, T. (2016) Role of a water network around the Mn_4CaO_5 cluster in photosynthetic water oxidation: a Fourier transform infrared spectroscopy and quantum mechanics/molecular mechanics calculation study. *Biochemistry* **55,** 597–607
88. Nakamura, S., and Noguchi, T. (2017) Infrared determination of the protonation state of a key histidine residue in the photosynthetic water oxidizing center. *J. Am. Chem. Soc.* **139,** 9364–9375
89. Kim, C. J., and Debus, R. J. (2017) Evidence from FTIR difference spectroscopy that a substrate H_2O molecule for O_2 formation in photosystem II is provided by the Ca ion of the catalytic Mn_4CaO_5 cluster. *Biochemistry* **56,** 2558–2570
90. Suzuki, H., Sugiura, M., and Noguchi, T. (2008) Monitoring water reactions during the S-state cycle of the photosynthetic water-oxidizing center: Detection of the DOD bending vibrations by means of Fourier transform infrared spectroscopy. *Biochemistry* **47,** 11024–11030
91. Isobe, H., Shoji, M., Shen, J.-R., and Yamaguchi, K. (2015) Strong coupling between the hydrogen bonding environment and redox chemistry during the S_2 to S_3 transition in the oxygen-evolving complex of photosystem II. *J. Phys. Chem. B* **119,** 13922–13933
92. Cox, N., Retegan, M., Neese, F., Pantazis, D. A., Boussac, A., and Lubitz, W. (2014) Electronic structure of the oxygen-evolving complex in photosystem II prior to O-O bond formation. *Science* **345,** 804–808
93. Capone, M., Narzi, D., Bovi, D., and Guidoni, L. (2016) Mechanism of water delivery to the active site of photosystem II along the S_2 to S_3 transition. *J. Phys. Chem. Lett.* **7,** 592–596
94. Hoganson, C. W., and Babcock, G. T. (1997) A metalloradical mechanism for the generation of oxygen from water in photosynthesis. *Science* **277,** 1953–1956
95. Rappaport, F., Blanchard-Desce, M., and Lavergne, J. (1994) Kinetics of electron transfer and electrochromic change during the redox transitions of the photosynthetic oxygen-evolving complex. *Biochim. Biophys. Acta* **1184,** 178–192
96. Haumann, M., Liebisch, P., Müller, C., Barra, M., Grabolle, M., and Dau, H. (2005) Photosynthetic O_2 formation tracked by time-resolved X-ray experiments. *Science* **310,** 1019–1021
97. Noguchi, T., Suzuki, H., Tsuno, M., Sugiura, M., and Kato, C. (2012) Time-resolved infrared detection of the proton and protein dynamics during photosynthetic oxygen evolution. *Biochemistry* **51,** 3205–3214
98. Stanier, R. Y., Kunisawa, R., Mandel, M., and Cohen-Bazire, G. (1971) Purification and properties of unicellular blue-green algae (order Chroococcales). *Bacteriol. Rev.* **35,** 171–205
99. Noguchi, T., Katoh, M., and Inoue, Y. (2002) A new system for detection of thermoluminescence and delayed luminescence from photosynthetic apparatus with precise temperature control. *Spectroscopy* **16,** 89–94